Arabian Journal of Chemistry (2017) **10**, S3559–S3568

King Saud University

Arabian Journal of Chemistry

www.ksu.edu.sa
www.sciencedirect.com

ORIGINAL ARTICLE

Quantum mechanical and multichannel RRKM studies of the reaction $N_2O + O(^3P)$

Fahimeh Shojaie

Department of Photonics, Graduate University of Advanced Technology, Kerman, Iran

Received 12 February 2013; accepted 2 March 2014
Available online 12 March 2014

KEYWORDS

Multichannel-RRKM;
Rate constants;
Dominant channel

Abstract The reaction of $N_2O + O(^3P) \rightarrow$ products is studied theoretically at 1000–5000 K, in this research two structures are used for N_2O: N=N=O (a) and N≡N–O (b). The detailed mechanism revealed for this time. The potential energy surface for this reaction has been investigated using CCSD (T) and CCSD (full) methods. The rate constants for feasible channels leading to five products were calculated by the multichannel-RRKM theory. The results show that at the temperatures higher than 2000 K, the dominant channel is $O(^3P) + N_2O \rightarrow 2NO$, while N_2O has structure (a) and at the temperatures lower than 2000 K; channel of $O(^3P) + N_2O \rightarrow N_2 + O_2$ is more favorable, while N_2O has structure (b).

1. Introduction

The reaction of oxygen atom O (^3P) with nitrous oxide (N_2O) has been studied considerably because of the importance of the reaction in the formation of NO_x pollutants during combustion (Brasseur et al., 1999). The O (^3P) + N_2O reaction has been investigated by many laboratories (Fontijn et al., 2000; Meagher and Anderson, 2000; Nishida et al., 2004]. Reasons for interest in this reaction and relevant references are presented in more detail in Refs. (Fontijn et al., 2000; Meagher and Anderson, 2000). This reaction can take place via two possible exothermic channels (Fontijn et al., 2000):

$$O(^3P) + N_2O\left(X^1\sum_g^+\right) \rightarrow NO(X^2\Pi) + NO(X^2\Pi) \quad (R1)$$

$$\rightarrow N_2\left(X^1\sum_g^+\right) + O_2\left(X^3\sum_g^+\right) \quad (R2)$$

The rate constant for reactions (R1) and (R2) has been measured in many studies and reported in the literatures. However the theoretical work is very limited for this reaction. To our knowledge, there is only one theoretical study about the reaction of O (^3P) with N_2O. In 2001, an ab initio study of the $3A''$ (under C_s symmetry) ground potential energy surface (PES) for this reaction has been performed at the CASPT2//CASSCF level (Gonzalwz et al., 2001). The rate constants were calculated by the Transition State Theory (TST) and this study shows that results for channel (R1) are almost in agreement with experiments. However, for channel (R2) there is a great discrepancy with experiments.

In this paper, first geometrical parameters, frequencies and energies of the reactants, intermediates, transition states and

E-mail address: fahimeh_shojaie@yahoo.com
Peer review under responsibility of King Saud University.

Production and hosting by Elsevier

http://dx.doi.org/10.1016/j.arabjc.2014.03.003

products for O (^{3}P) + N_2O reaction are calculated. In the second step, the kinetic calculations have been carried out using the multichannel RRKM (Rice–Ramsperger–Kassel–Marcus) (Holbrook et al., 1996) for total and individual rate constants. Several features of this work are following: (1) For N_2O (reactant) two structures (a) and (b) (N═N═O (a) and N═N═O (b)) are investigated. (2) The potential energy profile surface was calculated at the CCSD (T) (Pople et al., 1987) and CCSD (full) levels and Aug-cc-pVTZ (Kendall et al., 1992), 6-311 + + G (2df, 2pd) and 311 + + G (3df, 2p) basis sets. (3) The rate constants were obtained over a wide temperature range of 1000–5000 K, and the dominant products were studied. (4) The dependence of the reaction rate constants and branching ratios on the temperature is discussed.

2. Computation method

Ab initio calculation was carried out using Gauusian 03 programs (Frisch et al., 2004) and the geometries of the reactants, transition states, intermediates and products were optimized at the MP2 (Frisch et al., 1990)/full 6-311 + + G (2df, 2p) level. The vibrational frequencies were calculated at the same level of theory to determine the nature of different stationary points and the Zero-Point Energy (ZPE). All the stationary points have been positively identified for the minimum (number of imaginary frequencies NIMAG = 0) or transition states (NIMAG = 1). The intrinsic reaction coordinate (IRC) (Gonazales and Schlegel, 1990) calculation confirms that the transition state connects the designated reactions and products. To obtain more reliable energies higher levels, CCSD (T) and CCSD (full) and a more flexible basis set, Aug-cc-pVTZ, 6-311 + + G (2df, 2pd) and 311 + + G (3df, 2p), were employed to calculate the energies of various species.

3. Results and discussion

In this research, the mechanisms and kinetics of O (^{3}P) to N_2O were investigated by two structures (a) and (b) for N_2O. Fig. 1 shows the optimized geometries of all the stationary points at the MP2 (full)/6-311 + + G (2df, 2p) level of theory. The calculated relative energies at the different levels of theory and Zero-Point Energies (ZPEs) are listed in Table 1.

The reaction paths included in the calculation are shown in Fig. 2. Schematics of potential energy diagram at the CCSD (full)/6–311 + + G (2df, 2p) level of theory are presented in Fig. 3(R (a): O (^{3}P) + N_2O (a)). Vibrational term values and moments of inertia for all species are listed in Table 2.

4. Mechanism

As shown in Fig. 2, the reaction of N_2O with O (^{3}P) starts with the formation of the N_2O_2 when the oxygen atom attaches to the nitrogen atom in N_2O via transition state TS1 to form energized intermediate IM1. Starting from IM1, three different reaction paths are explored.

Path 1:

$$\begin{array}{l} \text{IM1}\rightarrow\text{TS2}\rightarrow\text{IM2}\rightarrow\ \text{TS3}\rightarrow\text{IM3}\rightarrow\ \text{P1 (2NO)} \\ \qquad\quad\downarrow \\ \qquad\quad\text{P1 (2NO)} \end{array} \qquad \text{(R3)}$$

In this path, IM1 can generate IM2 (NO···ON) via TS2, in TS2 the two 1N–3O and 4N–2O bonds are shortened by 0.101 and 0.109 Å, respectively, the 1N–4N bond is lengthened by 0.016 Å. The IM3 (NO···NO) is formed via TS3. The distances between atoms 2O–3O and 1N–4N increase from 2.100 and 2.140 Å in IM2 to 2.563 and 2.264 Å in TS3, respectively. As shown in Fig. 3, P1 was formed via IM3 by barrier less process.

Path 2:

$$\begin{array}{l} \qquad\qquad\text{P2 (N=N+O=O)} \\ \qquad\qquad\uparrow \\ \text{IM1}\rightarrow\text{TS4}\rightarrow\text{IM4}\rightarrow\text{TS5}\rightarrow\text{P3 (}N_2\text{+ }O_2\text{)} \qquad \text{(R4)} \\ \qquad\quad\searrow \\ \qquad\qquad\text{TS6}\rightarrow\text{IM5}\rightarrow\text{TS7}\rightarrow\text{IM6}\rightarrow\text{P5 (N=N +O-O)} \qquad \text{(R5)} \\ \qquad\qquad\qquad\qquad\downarrow \\ \qquad\qquad\qquad\qquad\text{P4 (}N_2\text{+ O-O)} \end{array}$$

This pathway proceeds by IM1 to form IM4 via TS4, in TS4 the lengths of bond 1N–3O increase to 1.674 Å and of 4N–2O to 1.561 Å, both bigger than in IM1, indicating almost complete breaking of these bonds. The IM4 may dissociate into N_2(S) + O_2(S) via channel IM4 → P3 (by TS5). Another possible path is formation of IM5 via TS6, in this channel the 1N–4N bond is shortened by 0.060 Å and the 2O–3O is lengthened by 0.132 Å. Then IM6 can be formed by TS7, in which the formation of 2O–3O bond is 1.354 Å, and the 1N–4N bond is lengthened by 0.064 Å. The P2, P4 and P5 were formed by barrier less process.

Path 3:

$$\text{IM1} \rightarrow \text{TS8} \rightarrow \text{P3}(N_2 + O_2) \qquad \text{(R6)}$$

The other reaction channel of IM1 is the direct decomposition of IM1 to the products N_2(S) and O_2(S) via transition state TS8. As shown in Fig. 1, the breaking of two 1N–3O and 4N–2O bonds of 1.430 and 1.422 Å are stretched by 0.322 and 0.330 Å, respectively, which indicates the TS8 should be very reactant-like, and thus the reaction has an early barrier. We were not able to reach a reasonable path for the formation of N_2(S) + 2O from N_2O + O (^{3}P).

5. Rate constant calculations

As it is shown in Fig. 3 the reaction of N_2O + O (^{3}P) can proceed via the saddle point TS1 leading to a common chemically activated intermediate (IM1). The various products originate from the unimolecular decomposition of this intermediate. In this research, the RRKM theory is used to calculate the rate constants for these products.

The individual rate constants for various product channels (R3–R6) are:

$$k_{\text{IM1}}(\text{T},\text{P}) = \frac{\alpha_a}{h}\frac{\text{Q}_\text{t}^+\text{Q}_\text{r}^+}{\text{Q}_{\text{N}_2\text{O}}\text{Q}_\text{O}} e^{-E_\text{a}/\text{RT}\Delta E^+}\sum_{i=1}^{i_{\max}}\frac{\omega}{Z}\text{N}_a(E^+)e^{-E^+/\text{RT}}$$

$$k_{\text{IM2}}(\text{T},\text{P}) = \frac{\alpha_a}{h}\frac{\text{Q}_\text{t}^+\text{Q}_\text{r}^+}{\text{Q}_{\text{N}_2\text{O}}\text{Q}_\text{O}} e^{-E_\text{a}/\text{RT}\Delta E^+}\sum_{i=1}^{i_{\max}}\frac{k_2\omega}{\text{Y}_1 Z}\text{N}_a(E^+)e^{-E^+/\text{RT}}$$

$$k_{\text{IM3}}(\text{T},\text{P}) = \frac{\alpha_a}{h}\frac{\text{Q}_\text{t}^+\text{Q}_\text{r}^+}{\text{Q}_{\text{N}_2\text{O}}\text{Q}_\text{O}} e^{-E_\text{a}/\text{RT}\Delta E^+}\sum_{i=1}^{i_{\max}}\frac{k_2 k_4\omega}{X_3\text{Y}_1 Z}\text{N}_a(E^+)e^{-E^+/\text{RT}}$$

Table 1 Relative energies of intermediates, transition states and products in the O (^3P) + N_2O reaction at various levels of theory and Zero Point Energies at the MP2 (full)/6-311++G (2df, 2p) level in kcal mol^{-1}.(R(a): O (^3P) + N_2O(a) and R(b): O (^3P) + N_2O(b)).

Species	Relative energy						ZPE
	CCSD (full) /Aug-cc-pVTZ	CCSD (full) /6-311++G (2df, 2pd)	CCSD (full) /6-311++G (3df, 2p)	CCSD (T) /6-311++G (2df, 2pd)	CCSD (T) /Aug-cc-pVTZ	CCSD (T) /6-311++G (3df, 2p)	MP2 (full) /6-311++G (2df, 2p)
R(a)	0.000	0.000	0.000	0.000	0.000	0.000	6.818
R(b)	0.000	0.000	0.000	0.000	0.000	0.000	3.694
IM1	22.427	26.243	25.643	18.409	15.100	17.486	7.631
	3.351	7.073	6.101	−0.518	−2.991	−1.574	
IM2	−10.656	−8.839	−10.005	−23.555	−25.456	−25.142	7.578
	−29.732	−28.009	−29.548	−42.484	−43.547	−44.203	
IM3	−3.931	−2.092	−3.445	−18.684	−20.558	−20.432	8.330
	−23.006	−21.262	−22.988	−37.613	−38.650	−39.492	
IM4	36.781	39.504	38.865	32.661	30.523	31.837	7.954
	17.705	20.334	19.322	13.733	12.431	12.776	
	−52.400	−51.559	−51.317	−58.111	−58.903	−57.973	
IM5	−33.325	−32.390	−31.774	−39.182	−40.811	−38.912	4.941
IM6	74.569	77.776	78.080	59.720	56.388	59.644	10.700
	55.493	58.606	58.537	40.792	38.296	40.583	
P1	−26.393	−26.328	−27.515	−25.852	−26.188	−27.206	13.693
	−45.469	−45.498	−47.058	−44.781	−44.280	−46.267	
P2	124.970	125.304	125.184	121.157	119.791	120.701	4.625
	105.895	106.134	105.641	102.228	101.699	101.640	
P3	−46.191	−45.252	−45.279	−47.376	−48.366	−47.612	5.279
	−65.267	−64.421	−64.822	−66.304	−66.458	−66.673	
P4	−67.202	−66.420	−65.989	−68.530	−69.944	−68.382	5.282
	−86.278	−85.590	−85.531	−87.459	−88.036	−87.443	
P5	103.959	104.135	104.474	100.003	98.213	99.931	4.625
	84.883	84.966	84.931	81.074	80.121	80.871	
TS1	61.927	66.455	65.122	58.573	55.676	57.175	8.214
	42.851	47.286	45.579	39.644	37.584	38.114	
TS2	40.743	44.118	42.792	30.798	28.189	29.169	6.896
	21.667	24.949	23.249	11.869	10.098	10.108	
TS3	31.904	34.946	32.756	19.586	18.483	17.391	8.344
	12.828	15.776	13.213	0.657	0.391	−1.669	
TS4	106.229	93.873	92.554	98.933	94.705	97.842	6.949
	87.153	74.704	73.011	80.004	76.613	78.781	
TS5	85.666	99.802	88.277	80.340	77.216	78.051	7.117
	66.590	80.632	68.734	61.411	59.124	58.990	
TS6	89.678	94.168	92.848	83.297	80.291	81.798	7.243
	70.603	74.998	73.306	64.368	62.199	62.737	
TS7	119.410	101.107	123.833	78.750	75.943	79.356	4.665
	100.334	81.937	104.290	59.821	57.851	60.295	
TS8	69.774	73.246	73.800	55.893	52.196	81.792	7.102
	50.698	54.076	54.257	36.964	34.104	62.732	

$$k_{\mathrm{IM4}}(\mathrm{T},\mathrm{P}k) = \frac{\alpha_a}{h}\frac{\mathrm{Q_t^+Q_r^+}}{\mathrm{Q_{N_2O}Q_O}} e^{-E_a/\mathrm{RT}\Delta E^+} \sum_{i=1}^{i_{\max}} \frac{k_6\omega}{Y_3 Z} \mathrm{N}_a(E^+) e^{-E^+/\mathrm{RT}}$$

$$k_{\mathrm{IM5}}(\mathrm{T},\mathrm{P}) = \frac{\alpha_a}{h}\frac{\mathrm{Q_t^+Q_r^+}}{\mathrm{Q_{N_2O}Q_O}} e^{-E_a/\mathrm{RT}\Delta E^+} \sum_{i=1}^{i_{\max}} \frac{k_6 k_9\omega}{Y_2 Y_3 Z} N_a(E^+) e^{-E^+/RT}$$

With the following definition:

$X_1 = k_1 + k_2 + k_6 + k_{13} + \omega$, $X_2 = k_3 + k_4 + \omega$, $X_3 = k_5 + \omega$,
$X_4 = k_7 + k_8 + k_9 + \omega$, $X_5 = k_{10} + k_{11} + \omega$, $X_6 = k_{12} + \omega$,

$Y_1 = X_2 - \frac{k_4 k_5}{X_3}$,, $Y_2 = X_5 - \frac{k_{11}k_{12}}{X_6}$, $Y_3 = X_4 - \frac{k_9 k_{10}}{Y_2}$, $Z = X_1 - \frac{k_2 k_3}{Y_1} - \frac{k_6 k_7}{Y_3}$,....., $E^+ = (i + \frac{1}{2})\Delta E^+$ $i = 0, 1, 2, 3, \ldots$, $E^+_{\max} = E_0 + sk_BT$, $k_{2\mathrm{NO}} = k_{\mathrm{IM2}} + k_{\mathrm{IM3}}$, $k_{\mathrm{N_2+O_2}} = k_{P3}$

In the above equations, α_a is the statistical factor (degeneracy) for the association step (Holbrook et al., 1996). $\mathrm{Q_t^+Q_r^+}$ are the translational and rotational partition function of the variational "transition state" for the association. $\mathrm{Q_{N_2O}Q_O}$ are the total partition function of N_2O and O, respectively. E_a is the barrier for the association. $\mathrm{N_a}(E^+)$ is the number of state for the association "transition state" and s is the number of active degrees of freedom. In addition, in the RRKM calculations, a step size of $\Delta E^+ = 0.8$ kJ mol^{-1}is used. The energy-specific rate constants are calculated using the RRKM theory as follows:

$$k_i(E) = \alpha_i \kappa_i C_i \frac{N_i(E_i^+)}{h\rho_j(E_j)}, i = 1, 2, \ldots, 8,\ j = 1, 2, \ldots, 6 \qquad \text{(R7)}$$

where α_i is the statistical factor for the ith reaction path, K_i is the tunneling factor that was considered using the Eckart

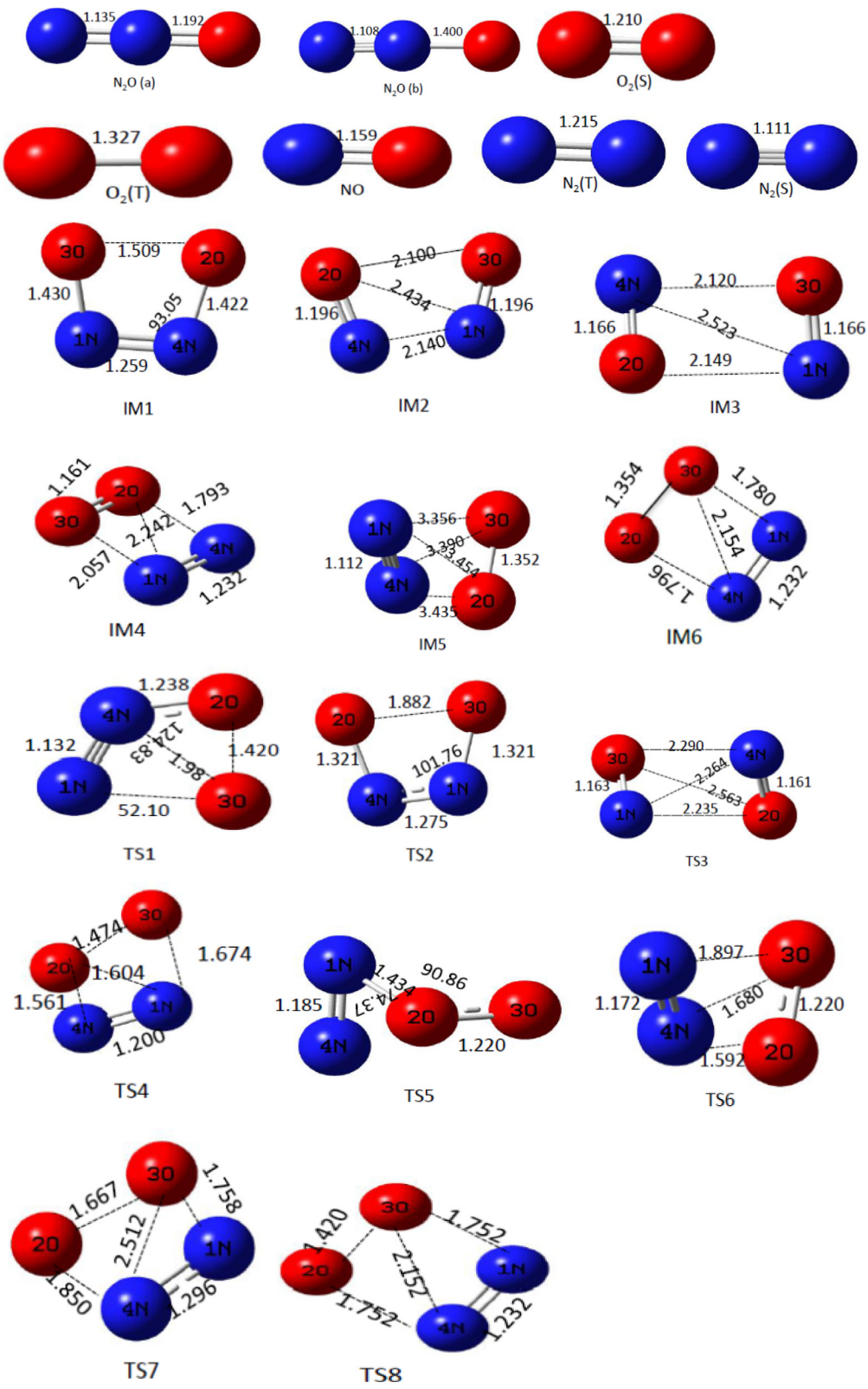

Figure 1 Optimized geometries of all the reactants, intermediates, transition states and products for the reaction of O (^{3}P) + N_2O at the MP2 (full)/6-311 + + G (2df, 2p). Bond lengths are in angstroms and angles are in degrees.

potential (Johnston and Heicklen, 1962), C_i is the ratio of the overall rotational partition function of the TSi (i = 1, 2,. . ., 8) and the intermediate IMj (1, 2, . . .,6), h is Planck's constant, $\rho_j(E_j)$ is the density of states at energy E of the intermediate j, $N_i(E_i^+)$ is the number of states at the energy above the barrier height E_i^+ for transition state i. The density of states and the

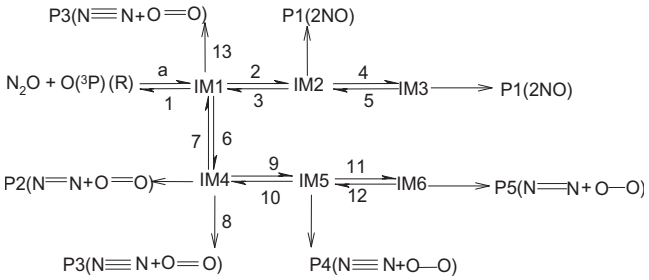

Figure 2 The reaction paths were included in the calculation for the reaction of O (^3P) + N_2O.

number of states are calculated using the Beyer–Swinehart algorithm (Stein and Rabinovitch, 1973; Astholz et al., 1979) The collision deactivation rate $\omega = \beta_c Z_{LJ}[He]$, where β_c is the collision efficiency calculated using Troe's weak collision

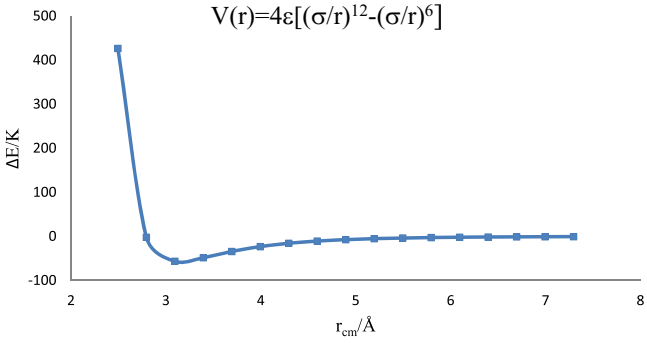

Figure 4 The MP2 (full)/6-311 + + G (2df, 2p) calculated intermolecular interaction energy between the IM1 and the helium bath gas. r_{cm} represents the separation of the center of mass of the IM1 and He.

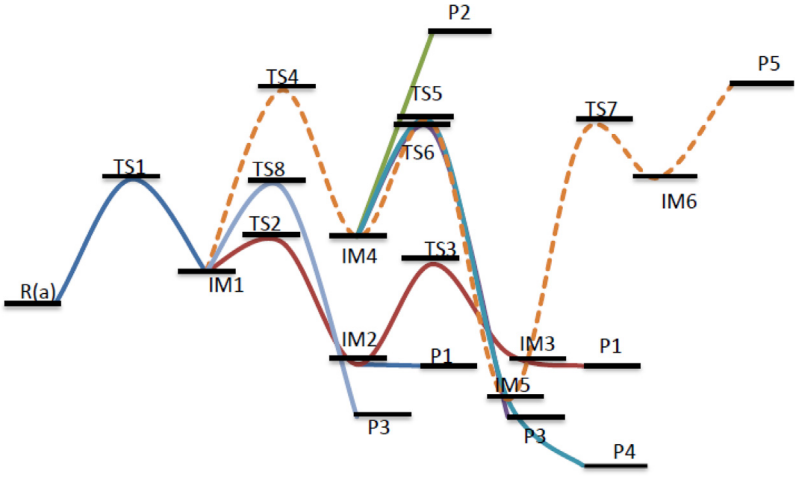

Figure 3 Schematic energy profile of the potential energy surface at the CCSD (full)/6-311 + + G (2df, 2p) level of theory (R (a): O (^3P) + N_2O (a)).

Table 2 Vibrational frequencies (cm^{-1}) and moments of inertia (amu) for various species for the O (^3P) + N_2O reaction at the MP2 = full/6-311 + + G (2df, 2 p) level of theory.

Species	I_a, I_b, I_c	Frequencies
N_2O(a)	144.90,144.90	602.0,602.0,1300.8,2264.4
N_2O(b)	0.01,169.47,169.48	234.5, 550.7, 2075.3
N_2(S)	30.87, 30.87	2201.9
N_2(T)	36.93, 36.93	1741.9
NO	35.81, 35.81	4789.2
O_2(S)	41.81, 41.81	1491.0
O_2(T)	50.29, 50.29	889.8
IM1	103.97, 108.40, 208.66	563.5, 668.6, 739.8, 927.9, 1047.7, 1390.1
IM2	76.37, 240.45, 316.82	399.2, 437.3, 510.6, 715.7, 1557.3, 1681.1
IM3	72.29, 243.18, 315.48	329.8, 434.8, 549.9, 683.6, 1786.9, 2042.7
IM4	75.53, 168.63, 274.16	152.0, 511.0, 710.5, 898.9, 1555.2, 1736.3
IM5	83.00, 609,06, 632.76	52.6, 57.4, 180.3, 280.7, 690.9, 2194.9
IM6	90.32, 170.32, 250.71	264.0, 600.3, 724.8, 1224.2, 1968.3, 2703.2
TS1	79.36, 157.42, 236.78	942.4i, 248.3, 794.3, 1046.2, 1417.9, 2239.2
TS2	87.93,141.85,225.58	1451.8i,684.0,878.0,1021.4,1052.8,1187.5
TS3	69.49, 279.57, 315.92	2678.6i,284.2,400.6,859.9,1836.3,2430.1
TS4	80.70,155.19,202.44	1022.6i,496.4,656.4,896.2,1102.9,1709.3
TS5	60.21,179.21,190.82	722.5i,427.2,638.6,690.0,1450.9,1772.0
TS6	71.66,168.14,192.58	1163.7i,312.7i,523.4,786.5,1686.4,1757.9
TS7	101.59,190.02,266.64	1513.4i,268.8,497.9,551.1,751.9,1193.9
TS8	95.53,163.35,249.03	1949.1i,444.6,657.8,678.6,1261.3,1925.6

Table 3 Calculated rate constants ($cm^3molecule^{-1}s^{-1}$) for the N_2O + O (^3P) reaction in the temperature range 2000–5000 K.

T(K)	kIM1		kIM2		kIM3		kIM4		kIM5		kIM6		$k_{N_2+O_2} = k$P3		K_{2NO}		$k_{N_2+O_2}$	K_{2NO}
	R(a)	R(b)	R(a)	R(b)	R(a)	R(b)	R(a)	R(b)	R(a)	R(b)	R(a)	R(b)	R(a)	R(b)	R(a)	R(b)		
1000	1.15E-20	1.10E-16	2.66E-21	2.66E-17	1.24E-22	1.30E-18	3.16E-22	3.16E-18	5.12E-24	5.39E-20	4.56E-29	5.03E-25	1.27E-21	1.27E-17	2.78E-21	2.79E-17	2.02E-15[a]	1.36E-16[a]
	1.35E-20	1.30E-16	3.26E-21	3.30E-17	1.42E-22	1.45E-18	4.98E-22	5.02E-18	7.68E-24	8.14E-20	8.05E-29	8.95E-25	1.58E-21	1.59E-17	3.40E-21	3.44E-17	1.60E-19[b]	1.36E-16[b]
	2.03E-20	2.60E-16	5.03E-21	6.79E-17	2.28E-22	3.24E-18	7.66E-22	1.04E-17	3.43E-24	4.89E-20	2.99E-29	4.50E-25	2.23E-21	3.02E-17	5.26E-21	7.11E-17		
	3.23E-19	2.64E-15	1.35E-19	1.18E-15	6.31E-21	5.84E-17	9.75E-21	8.49E-17	4.87E-23	4.52E-19	5.91E-28	5.83E-24	5.43E-20	4.73E-16	1.42E-19	1.23E-15		
	1.19E-18	6.39E-15	4.83E-19	2.58E-15	2.17E-20	8.47E-17	3.68E-20	2.11E-16	1.90E-22	1.17E-18	2.39E-27	1.56E-23	1.99E-19	1.14E-15	5.05E-19	2.67E-15		
	2.00E-19	3.13E-15	1.04E-19	1.61E-15	5.24E-21	8.10E-17	6.28E-21	9.78E-17	1.24E-22	1.91E-18	1.76E-27	2.70E-23	1.58E-20	2.47E-16	1.09E-19	1.69E-15		
1500	5.12E-16	1.60E-13	1.71E-16	5.72E-14	1.01E-17	3.65E-15	2.07E-17	6.96E-15	5.05E-19	1.83E-16	6.13E-24	2.38E-21	8.37E-17	2.82E-14	1.81E-16	6.08E-14	2.92E-14[a]	1.41E-14[a]
	5.49E-16	1.75E-13	1.91E-16	6.53E-14	1.11E-17	4.09E-15	2.98E-17	1.02E-14	7.05E-19	2.61E-16	1.01E-23	4.00E-21	8.87E-17	3.05E-14	2.02E-16	6.94E-14	1.59E-16[b]	1.15E-14[b]
	6.94E-16	1.51E-13	2.67E-16	6.29E-14	1.55E-17	3.95E-15	4.04E-17	9.55E-15	2.88E-19	7.38E-17	3.43E-24	9.51E-22	1.13E-16	2.68E-14	2.83E-16	6.69E-14		
	3.42E-15	1.11E-13	2.20E-15	7.78E-14	1.32E-16	5.14E-15	1.54E-16	5.47E-15	1.24E-18	4.87E-17	2.11E-23	9.07E-22	8.10E-16	2.89E-14	2.33E-15	8.30E-14		
	7.58E-15	1.06E-13	4.37E-15	6.74E-14	2.56E-16	4.36E-15	3.50E-16	5.42E-15	2.86E-18	4.92E-17	4.96E-23	9.35E-22	2.94E-15	2.86E-14	4.63E-15	7.17E-14		
	1.66E-15	2.50E-13	1.20E-15	1.86E-13	7.89E-17	1.26E-14	7.91E-17	1.23E-14	2.28E-18	3.65E-16	4.53E-23	7.49E-21	1.86E-16	2.88E-14	1.28E-15	1.98E-13		
2000	9.21E-14	4.51E-13	4.60E-14	2.46E-13	3.64E-15	2.14E-14	5.21E-15	2.80E-14	1.90E-16	1.13E-15	3.09E-21	2.01E-20	2.12E-14	1.15E-13	4.96E-14	2.68E-13	1.11E-13[a]	1.44E-13[a]
	9.51E-14	4.07E-13	4.97E-14	2.34E-13	3.70E-15	1.91E-14	7.46E-15	3.51E-14	2.57E-16	1.34E-15	4.89E-21	2.79E-20	2.25E-14	1.07E-13	5.34E-14	2.53E-13	5.63E-15[b]	1.22E-13[b]
	1.14E-13	4.47E-13	6.14E-14	2.67E-13	4.90E-15	2.36E-14	9.45E-15	4.14E-14	9.48E-17	4.62E-16	1.52E-21	8.18E-21	2.54E-14	1.11E-13	6.63E-14	2.90E-13		
	1.48E-13	2.74E-13	1.31E-13	2.74E-13	1.06E-14	2.51E-14	9.71E-15	2.04E-14	1.11E-16	2.66E-16	2.48E-21	6.63E-21	5.23E-14	1.10E-13	1.42E-13	2.99E-13		
	1.56E-13	2.65E-13	1.35E-13	2.59E-13	1.06E-14	2.31E-14	1.06E-14	2.05E-14	1.27E-16	2.81E-16	2.95E-21	7.37E-21	5.54E-14	1.08E-13	1.45E-13	2.82E-13		
	1.16E-13	6.33E-13	1.24E-13	7.20E-13	1.07E-14	6.65E-14	7.78E-15	4.52E-14	2.95E-16	1.84E-15	8.24E-21	5.51E-20	1.87E-14	1.10E-13	1.35E-13	7.87E-13		
2500	7.91E-13	6.96E-13	5.19E-13	5.10E-13	5.31E-14	5.85E-14	5.89E-14	5.80E-14	2.89E-15	3.22E-15	5.95E-20	7.42E-20	2.50E-13	2.49E-13	5.72E-13	5.68E-13	2.48E-13[a]	5.78E-13[a]
	7.84E-13	6.91E-13	5.14E-13	5.08E-13	4.97E-14	5.51E-14	8.03E-14	7.93E-14	3.81E-15	4.27E-15	9.20E-20	1.15E-19	2.46E-13	2.46E-13	5.64E-13	5.63E-13	5.09E-14[b]	5.41E-13[b]
	6.96E-13	6.82E-13	5.00E-13	5.52E-13	5.01E-14	6.26E-14	7.93E-14	8.84E-14	1.13E-15	1.44E-15	2.29E-20	3.30E-20	2.19E-13	2.46E-13	5.50E-13	6.14E-13		
	4.29E-13	4.45E-13	4.94E-13	5.91E-13	5.22E-14	7.24E-14	3.76E-14	4.55E-14	6.16E-16	8.77E-16	1.78E-20	2.89E-20	2.02E-13	2.46E-13	5.47E-13	6.64E-13		
	4.82E-13	4.03E-13	5.12E-13	4.97E-13	5.31E-14	6.00E-14	4.38E-14	4.30E-14	7.36E-16	8.55E-16	2.18E-20	2.91E-20	2.36E-13	2.34E-13	5.65E-13	5.57E-13		
	4.00E-13	1.05E-12	5.14E-13	1.48E-12	6.12E-14	1.96E-13	3.62E-14	1.05E-13	1.83E-15	5.87E-15	6.75E-20	2.40E-19	8.62E-14	2.52E-13	5.75E-13	1.68E-12		
3000	1.61E-12	8.38E-13	1.33E-12	7.88E-13	1.67E-13	1.13E-13	1.53E-13	9.07E-14	1.03E-14	7.04E-15	2.67E-19	2.08E-19	6.69E-13	4.05E-13	1.50E-12	9.01E-13	4.23E-13[a]	1.46E-12[a]
	1.47E-12	8.67E-13	1.27E-12	8.54E-13	1.57E-13	1.20E-13	1.99E-13	1.33E-13	1.22E-14	9.52E-15	3.67E-19	3.23E-19	6.31E-13	4.32E-13	1.43E-12	9.74E-13	2.29E-13[b]	1.53E-12[b]
	1.57E-12	8.59E-13	1.40E-12	8.80E-13	1.84E-13	1.34E-13	2.34E-13	1.49E-13	4.31E-15	3.23E-15	1.10E-19	9.49E-20	6.34E-13	4.09E-13	1.58E-12	1.01E-12		
	9.32E-13	5.09E-13	1.32E-12	8.48E-13	1.79E-13	1.36E-13	1.10E-13	7.17E-14	2.34E-15	1.85E-15	8.21E-20	7.52E-20	6.05E-13	4.00E-13	1.50E-12	9.84E-13		
	8.90E-13	5.04E-13	1.24E-12	8.29E-13	1.64E-13	1.31E-13	1.09E-13	7.42E-14	2.45E-15	2.04E-15	9.03E-20	8.74E-20	5.87E-13	4.05E-13	1.40E-12	9.60E-13		
	7.66E-13	1.19E-12	1.26E-12	2.20E-12	1.96E-13	3.91E-13	8.99E-14	1.58E-13	5.57E-15	1.12E-14	2.73E-19	6.31E-19	2.25E-13	4.02E-13	1.46E-12	2.59E-12		
3500	2.47E-12	9.43E-13	2.46E-12	1.08E-12	3.94E-13	2.00E-13	2.91E-13	1.27E-13	2.45E-14	1.28E-14	7.67E-19	4.59E-19	1.33E-12	6.04E-13	2.85E-12	1.28E-12	6.20E-13[a]	2.84E-12[a]
	2.54E-12	9.76E-13	2.54E-12	1.13E-12	3.86E-13	2.00E-13	4.16E-13	1.85E-13	3.40E-14	1.79E-14	1.22E-18	7.38E-19	1.39E-12	6.39E-13	2.92E-12	1.33E-12	6.90E-13[b]	3.30E-12[b]
	2.34E-12	9.78E-13	2.53E-12	1.24E-12	3.99E-13	2.29E-13	4.46E-13	2.22E-13	1.06E-14	6.34E-15	3.26E-19	2.28E-19	1.25E-12	6.31E-13	2.93E-12	1.47E-12		
	1.39E-12	6.42E-13	2.33E-12	1.29E-12	3.92E-13	2.62E-13	2.05E-13	1.16E-13	5.68E-15	4.00E-15	2.43E-19	1.99E-19	1.13E-12	6.51E-13	2.72E-12	1.55E-12		
	1.57E-12	6.01E-13	2.48E-12	1.14E-12	4.12E-13	2.31E-13	2.42E-13	1.14E-13	7.14E-15	4.22E-15	3.15E-19	2.18E-19	1.34E-12	6.44E-13	2.89E-12	1.38E-12		
	1.29E-12	1.37E-12	2.38E-12	2.87E-12	4.72E-13	6.73E-13	1.92E-13	2.35E-13	1.50E-14	2.17E-14	9.28E-19	1.58E-18	4.83E-13	6.06E-13	2.85E-12	3.54E-12		

4000	3.41E-12	9.64E-13	3.99E-12	1.32E-12	7.52E-13	2.91E-13	4.84E-13	1.59E-13	5.28E-14	2.10E-14	2.00E-18	9.26E-19	2.31E-12	7.94E-13	4.74E-12	1.61E-12	8.25E-13[a]	4.67E-12[a]
	3.27E-12	9.70E-13	3.98E-12	1.38E-12	7.50E-13	3.07E-13	6.64E-13	2.30E-13	6.69E-14	2.81E-14	2.85E-18	1.38E-18	2.27E-12	8.22E-13	4.73E-12	1.69E-12	1.61E-12[b]	6.02E-12[b]
	3.21E-12	1.05E-12	4.05E-12	1.57E-12	7.96E-13	3.67E-13	7.62E-13	3.02E-13	2.29E-14	1.12E-14	8.49E-19	4.89E-19	2.11E-12	8.54E-13	4.84E-12	1.94E-12		
	2.02E-12	6.51E-13	3.91E-12	1.53E-12	8.02E-13	3.85E-13	3.80E-13	1.53E-13	1.34E-14	6.88E-15	6.59E-19	3.96E-19	2.14E-12	8.82E-13	4.71E-12	1.91E-12		
	2.01E-12	5.64E-13	3.83E-12	1.32E-12	7.77E-13	3.31E-13	3.93E-13	1.39E-13	1.47E-14	6.72E-15	7.64E-19	4.10E-19	2.23E-12	8.10E-13	4.61E-12	1.65E-12		
	1.68E-12	1.36E-12	3.68E-12	3.44E-12	9.11E-13	1.03E-12	3.09E-13	2.93E-13	2.85E-14	3.29E-14	2.25E-18	3.15E-18	8.17E-13	8.07E-13	4.59E-12	4.47E-12		
4500	4.20E-12	1.02E-12	5.62E-12	1.61E-12	1.28E-12	4.36E-13	7.03E-13	1.99E-13	9.30E-14	3.26E-14	4.08E-18	1.68E-18	3.54E-12	1.06E-12	6.90E-12	2.04E-12	1.03E-12[a]	6.88E-12[a]
	4.19E-12	6.84E-13	5.65E-12	1.09E-12	1.23E-12	2.85E-13	1.96E-11	3.77E-12	2.51E-12	5.96E-13	1.23E-16	3.38E-17	5.08E-12	1.08E-12	6.88E-12	1.38E-12	3.15E-12[b]	9.76E-12[b]
	3.65E-12	1.06E-12	5.50E-12	1.91E-12	1.24E-12	5.18E-13	1.06E-12	3.78E-13	3.94E-14	1.76E-14	1.70E-18	9.04E-19	2.97E-12	1.08E-12	6.74E-12	2.43E-12		
	2.47E-12	6.66E-13	5.38E-12	1.79E-12	1.31E-12	5.40E-13	5.67E-13	1.94E-13	2.49E-14	1.11E-14	1.40E-18	7.33E-19	3.15E-12	1.11E-12	6.70E-12	2.33E-12		
	2.64E-12	5.63E-13	5.48E-12	1.45E-12	1.33E-12	4.41E-13	6.24E-13	1.70E-13	2.93E-14	1.05E-14	1.73E-18	7.35E-19	3.55E-12	1.00E-12	6.81E-12	1.89E-12		
	2.29E-12	1.41E-12	5.33E-12	3.84E-12	1.63E-12	1.46E-12	5.10E-13	3.75E-13	5.72E-14	5.25E-14	5.52E-18	6.31E-18	1.37E-12	1.06E-12	6.96E-12	5.30E-12		
5000	4.93E-12	9.20E-13	7.41E-12	1.65E-12	1.97E-12	5.22E-13	9.94E-13	2.18E-13	1.64E-13	4.52E-14	8.73E-18	2.85E-18	5.02E-12	1.18E-12	9.38E-12	2.17E-12	1.23E-12[a]	9.37E-12[a]
	4.73E-12	9.46E-13	7.41E-12	1.77E-12	1.92E-12	5.53E-13	1.32E-12	3.11E-13	2.05E-13	6.10E-14	1.13E-17	3.90E-18	4.95E-12	1.26E-12	9.34E-12	2.33E-12	5.46E-12[b]	1.46E-11[b]
	4.53E-12	9.85E-13	7.35E-12	1.93E-12	1.99E-12	6.34E-13	1.58E-12	4.27E-13	7.15E-14	2.48E-14	3.25E-18	1.35E-18	4.50E-12	1.26E-12	9.34E-12	2.57E-12		
	3.08E-12	5.44E-13	7.46E-12	1.64E-12	2.08E-12	5.72E-13	8.51E-13	1.94E-13	4.58E-14	1.39E-14	2.93E-18	1.04E-18	4.90E-12	1.16E-12	9.53E-12	2.22E-12		
	5.75E-12	2.79E-13	7.18E-12	2.05E-12	2.04E-12	7.35E-13	1.35E-12	1.59E-13	7.76E-14	1.23E-14	5.04E-18	9.58E-19	6.51E-12	1.25E-12	9.22E-12	2.79E-12		
	2.65E-12	1.29E-12	6.95E-12	4.00E-12	2.56E-12	1.87E-12	6.75E-13	3.97E-13	1.09E-13	8.18E-14	1.30E-17	1.25E-17	1.98E-12	1.25E-12	9.51E-12	5.87E-12		

[a] Determined according to the expression: $k_{2NO} = 1.52 \times 10^{-10} \exp(-13930/T)$ and $k_{N_2+O_2} = 6.13 \times 10^{-12} \exp(-8020/T)$ cm^3 molecule^{-1} s^{-1} (Ref. Curtiss et al., 1991).
[b] Ref. Curtiss et al., 1998.

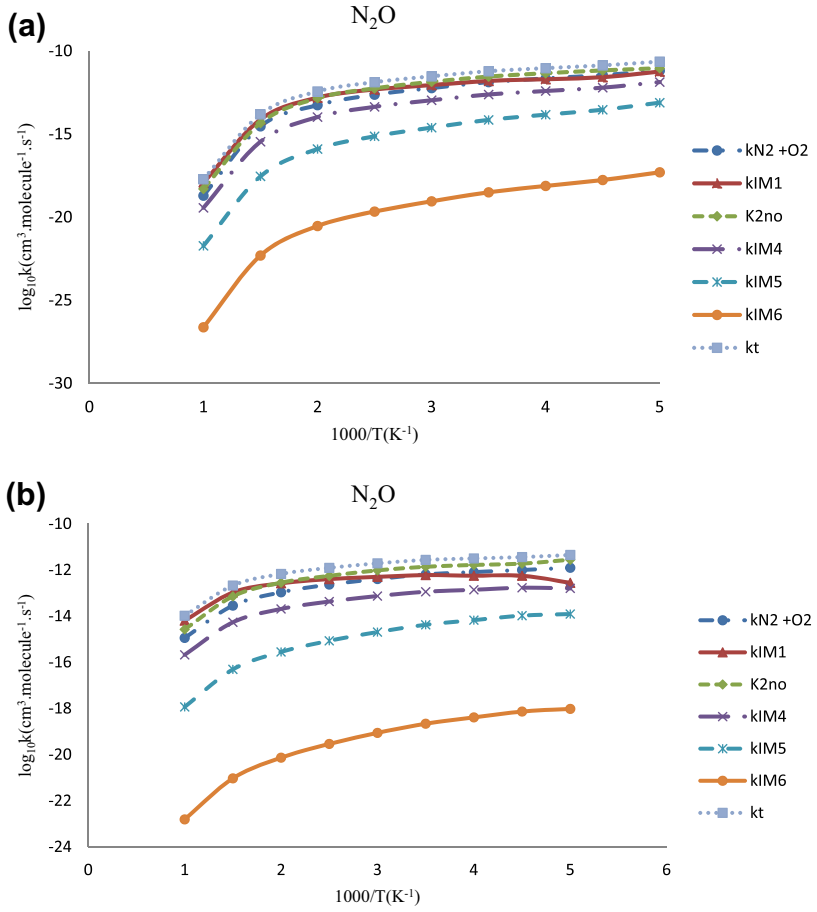

Figure 5 The logarithm of calculated rate constants as a function of $10^3/T$ for the O (^{3}P) + N_2O reaction for two structures of N_2O N═N═O (a) and N≡N─O (b)).

Table 4 Calculated enthalpies of reaction at the G1, G2, G3, G2MP2 and CBS-QB3 levels in kcal mol^{-1}.

Reaction	G1	G2	G3	G2MP2	CBS-QB3	Exp[a]
$O + N_2O \rightarrow NO + NO$	−37.77	−38.82	−36.55	−39.54	−37.06	−36.0
	−56.02	−57.29	−55.77	−58.13	−57.30	
$O + N_2O \rightarrow N_2 + O_2$	−48.61	−47.79	−49.11	−47.76	−49.28	−79.6
	−69.04	−68.44	−68.33	−68.52	−69.52	

[a] Ref. (Meagher and Anderson, 2000).

approximation (Troe, 1977) with the energy transfer parameter $-\langle\Delta E\rangle$. This parameter is unknown and cannot be calculated quantitatively. In consideration of the experimental rate constants, it is found that the values 20 cm^{-1} for $-\langle\Delta E\rangle$ should be reasonable to calculate the rate constants. Z_{LJ} is the Lennard–Jones collision frequency. [He] is the concentration of the helium bath gas. The weak collision approximation is used for each intermediate and the collisional rates are assumed to be the same for all intermediates for simplicity (Marchand et al., 1998). The collision efficiency is estimated using the Lennard–Jones potential by fitting the interaction energies calculated at the MP2 = full/6-311 + G (2df, 2p) level for IM1···He, and the potential well (ε = 56.840 K) and the collisional diameter (σ = 2.79 Å) are estimated (Fig. 4).

The RRKM calculations have been performed for both (a) and (b) conformations. Table 3 shows the individual rate constants over the temperature range of 1000–5000 K, at a pressure of 760 Torr and at the CCSD (T) and CCSD (full) levels and Aug-cc-pVTZ, 6-311++G (2df, 2pd) and 311++G (3df, 2p) basis sets, in comparison with the experimental results (Meagher and Anderson, 2000) and Ref. (Gonzalwz et al., 2001). In addition, Fig. 5 shows that the main products are 2NO, N_2 + O_2 and IM1, in both structure of (a) and (b). Also, From Figs. 2 and 3, we can see the decomposition of IM1 to yield 2NO and N_2 + O_2, thus the main channels are R (1) and R (2).

Table 3 indicates that at 1000 and 2000 K reaction rate of R(1) (k_{2NO}) and reaction rate of R(2) ($k_{N_2+O_2}$)for structure

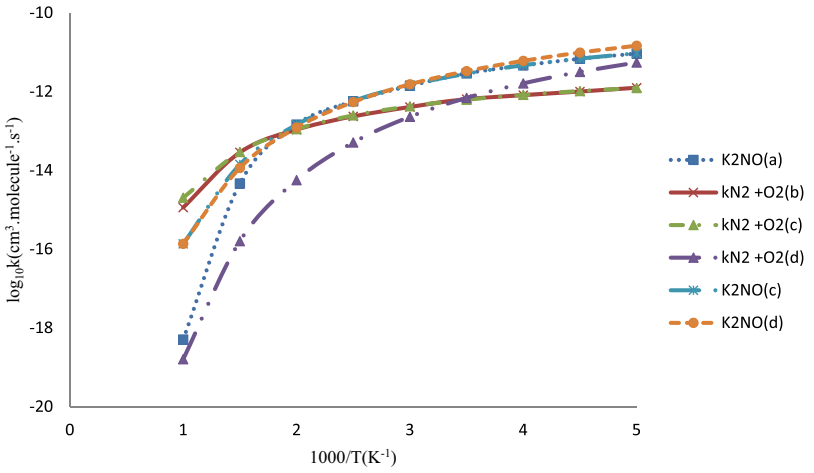

Figure 6 The logarithm of calculated rate constants as a function of $10^3/T$ for the O (^3P) + N_2O reaction. [a]Calculations with structure of N═N═O (a), [b]Calculations with structure of N≡N─O (b), [c]Ref. (Meagher and Anderson, 2000). [d]Ref. (Nishida et al., 2004).

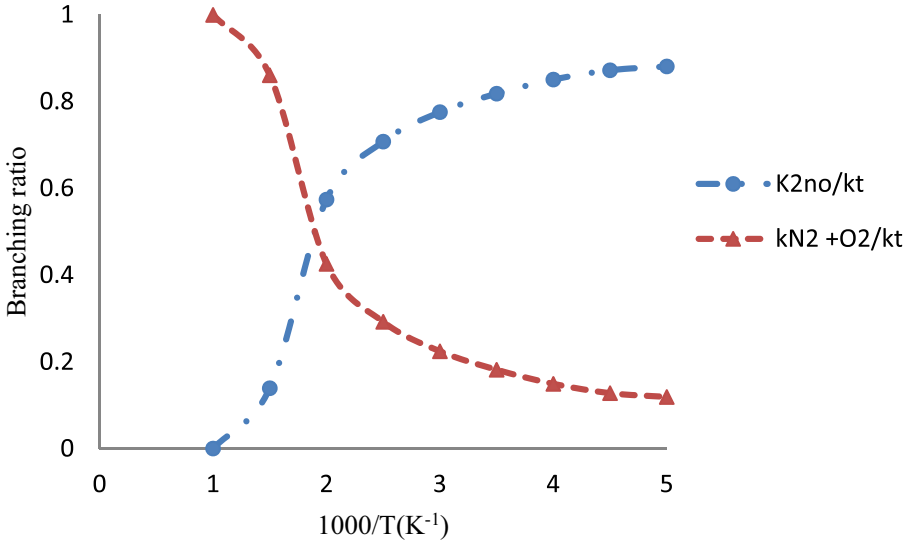

Figure 7 The calculated branching ratio for the reaction of O (^3P) + N_2O as a function of T (K), for two structures of N═N═O (a) and N≡N─O (b).

of (b) are in better agreement with available experimental value especially at the CCSD (T) level and Aug-cc-pVTZ, 6-311 + + G (2df, 2pd) and 311 + + G (3df, 2p) basis sets. Above 2000 K, the values of k_{2NO} for structure of (a) and the values of $(k_{N_2+O_2})$for structure of (b) are in excellent agreement with available experimental values at different levels. In addition, the enthalpies of reaction paths for the formation of (a) and (b) at 298 K were calculated at the G1 (Pople et al., 1989; Curtiss et al., 1990) G2 (Curtiss et al., 1991), G3 (Curtiss et al., 1998), G2MP2 (Curtiss et al., 1993) and CBS-QB3 (Montgomery et al., 1999) levels of theory. These values are presented in Table 4 and compared with the experimental data. The values predicted by these levels show enthalpies of 2NO reaction for (a) and N_2 + O_2 reaction for (b) are in better agreement with available experimental data.

Therefore this reaction is dominated by two different reaction channels: channel O (^3P) + $N_2O \rightarrow$ 2NO (R1), while N_2O has structure N═N═O and channel O (^3P) + $N_2O \rightarrow N_2$ + O_2 (R2) while N_2O has structure N≡N–O, these results match excellently with the experimental values and are shown in Fig. 6. Also, because of rate constants great discrepancies with experimental values for channel R (2) in Ref. (Curtiss et al., 1998) have been shown by these results. The branching ratios shown in Fig. 7 indicate that the major product is 2NO at temperature higher than 2000 K, while N_2 + O_2 is domain channel at temperature lower than 2000 K.

6. Conclusions

In this research, the multichannel-RRKM theory is employed to calculate the rate coefficients for the N_2O + O (^3P) reaction over the temperature range of 1000–5000 K. Various electronic structure theories were used to compute the energies of the stationary points on the potential energy surface of the reaction

that lead to two major products. The results show the major channels are the addition of O to N_2O leading to an intermediate N_2O_2, which then decomposes to 2NO and $N_2 + O_2$, thus this reaction has two important product channels: 2NO and $N_2 + O_2$. The results show that at the temperatures higher than 2000 K, the formation of 2NO is the dominant channel, while N_2O has structure N═N═O, and at the temperatures lower than 2000 K, the formation of $N_2 + O_2$ is more favorable while N_2O has structure N≡N–O. These results match with the experimental values.

Acknowledgments

This work was supported by Graduate University of Advanced Technology and Research Center for Science, High Technology & Environmental Science, Kerman, Iran.

References

Astholz, D.C., Troe, J., Wieters, W., 1979. Unimolecular processes in vibrationally highly excited cycloheptatrienes. I. Thermal isomerization in shock waves. J. Chem. Phys. 70, 5107–5116.

Brasseur, G.P., Orlando, J.J., Tyndall, G.S., 1999. Atmospheric Chemistry and Global Change. Oxford University Press, New York.

Curtiss, L.A., Jones, C., Trucks, G.W., Raghavachari, K., Pople, J.A., 1990. Gaussian-1 theory of molecular energies for second-row compounds. J. Chem. Phys. 93, 2537–2545.

Curtiss, L.A., Raghavachari, K., Trucks, G.W., Pople, J.A., 1991. Gaussian-2 theory for molecular energies of first- and second-row compounds. J. Chem. Phys. 94, 7221–7230.

Curtiss, L.A., Raghavachari, K., Pople, J.A., 1993. Gaussian-2 theory using reduced Møller–Plesset orders. J. Chem. Phys. 98, 1293–1298.

Curtiss, L.A., Raghavachari, K., Redfern, P.C., Rassolov, V., Pople, J.A., 1998. Gaussian-3 (G3) theory for molecules containing first and second-row atoms. J. Chem Phys. 109, 7764–7776.

Fontijn, A., Goumri, A., Fernandez, A., Anderson, W.R., Meagher, N.E., 2000. Kinetics of the O (3P) + N_2O reaction. 1. Direct measurements at intermediate temperatures. J. Phys. Chem. A 104, 6003–6012.

Frisch, M.J., Head-Gordon, M., Pople, J.A., 1990. Semi-direct algorithms for the MP2 energy and gradient. Chem. Phys. Lett. 166, 281–289.

Frisch, M.J., Trucks, G.W., Schlegel, H.B., Gill, P.M.W., Johnson, B.G., Robb, M.A., Cheeseman, J.R., Keith, T., Petersson, G.A., Montgomery, J.A., Raghavachari, K., Al-Laham, M.A., Zakrzewski, V.G., Ortiz, J.V., oresman, J.B., Cioslowski, J., Stefanov, B.B., Nanayakkara, A., Challacombe, M., Peng, C.Y., Ayala, P.Y., Chen, W., Wong, M.W., Andres, J.L., Replogle, E.S., Gomperts, R., Martin, R.L., Fox, D.J., Binkley, J.S., Defrees, D.J., Baker, J., Stewart, J.P., Head-Gordon, M., Gonzalez, C., Pople, J.A., 2004. Gaussian 03, revision C.01, Gaussian Inc, wallingford, CT.

Gonazales, C., Schlegel, H.B., 1990. Reaction path following in mass-weighted internal coordinates. J. Chem. Phys. 94, 5523–5527.

Gonzalwz, M., Valero, R., Sayos, R., 2001. Ab initio ground potential energy surface (3A″) for the O(3P)+N2O reaction and kinetics study. J. Chem. Phys. 115, 2540–2549.

Holbrook, K.A., Pilling, M.J., Robertson, S.H., 1996. Unimolecular Reactions. John Wiley & Sons, Chichester, UK.

Johnston, H.S., Heicklen, J., 1962. Tunneling corrections for unsymmetrical Eckart potential energy barriers. J. Phys. Chem. 66, 532–533.

Kendall, R.A., Dunning Jr., T.H., Harrison, R.J., 1992. Electron affinities of the first-row atoms revisited. Systematic basis sets and wave functions. J. Chem. Phys. 96, 6796–6806.

Marchand, N., Rayez, J.C., Smith, S.C., 1998. Theoretical study of the reaction CH(X2Π) + NO(X2Π). 3. Determination of the branching ratios. J. Phys. Chem. A 102, 3358–3367.

Meagher, N.E., Anderson, W.R., 2000. Kinetics of the O (^{3}P) + N_2O Reaction. 2. Interpretation and Recommended Rate Coefficients. J. Phys. Chem. A 104, 6013–6031.

Montgomery Jr., J.A., Frisch, M.J., Ochterski, J.W., Petersson, G.A., 1999. A complete basis set model chemistry. VI. Use of density functional geometries and frequencies. J. Chem. Phys. 110, 2822–2827.

Nishida, S., Takahashi, K., Matsumi, Y., Taniguchi, N., Hayashida, S., 2004. J. Phys. Chem. A 108, 2451.

Pople, J.A., Head-Gordon, M., Raghavachari, K., 1987. Quadratic configuration interaction. A general technique for determining electron correlation energies. J. Chem. Phys. 87, 5968–5975.

Pople, J.A., Head-Gordon, M., Fox, D.J., Raghavachari, K., Curtiss, L.A., 1989. Gaussian-1 theory: a general procedure for prediction of molecular energies. J. Chem. Phys. 90, 5622–5629.

Stein, S.E., Rabinovitch, B.S., 1973. Accurate evaluation of internal energy level sums and densities including anharmonic oscillators and hindered rotors. J. Chem. Phys. 58, 2438–2443.

Troe, J., 1977. Theory of thermal unimolecular reactions at low pressures. I. Solutions of the master equation. J. Chem. Phys. 66, 4745–4758.